Journal of Photochemistry and Photobiology A: Chemistry 232 (2012) 1–7

Contents lists available at SciVerse ScienceDirect

Journal of Photochemistry and Photobiology A: Chemistry

journal homepage: www.elsevier.com/locate/jphotochem

Cr modified TiO_2-loaded MCM-41 catalysts for UV-light driven photodegradation of diethyl sulfide and ethanol

P.A. Kolinko[a,b], P.G. Smirniotis[c,*], D.V. Kozlov[a,b], A.V. Vorontsov[a,b,**]

[a] Boreskov Institute of Catalysis, Novosibirsk 630090, Russia
[b] Novosibirsk State University, Novosibirsk 630090, Russia
[c] Department of Chemical and Materials Engineering, University of Cincinnati, Cincinnati, OH 45221-0012, USA

ARTICLE INFO

Article history:
Received 18 September 2011
Received in revised form 17 January 2012
Accepted 21 January 2012

Keywords:
MCM
Transition metal doping
Titanium dioxide
Diethyl sulfide
Ethanol
CWA
Photocatalytic oxidation
Visible light

ABSTRACT

Gas-phase photocatalytic oxidation (PCO) and adsorption of diethyl sulfide and ethanol in a batch reactor using Cr-modified TiO_2-loaded MCM-41 silica and commercial TiO_2 as photocatalysts were studied with in situ FTIR method. Mesoporous molecular sieves MCM-41 modified with Cr were synthesized by hydrothermal method; Si:Cr atomic ratio was 80:1 or 20:1. Final deposition of 25% TiO_2 was conducted by sol-gel method using titanium isopropoxide as a precursor. Adsorption measurements in a static reactor were used to estimate the Langmuir isotherm parameters (monolayer capacity and adsorption constant). Photooxidation experiments under UV irradiation demonstrated that TiO_2 loading on Cr-MCM-41 improve its activity in diethyl sulfide removal but decelerated the CO_2 formation. On the contrary, the rate of ethanol oxidation increased strongly as a result of TiO_2 loading and the highest activity was observed for 25% TiO_2/MCM-41 photocatalyst without chromium. Sulfate species were detected on the TiO_2 surface after complete diethyl sulfide oxidation. Water and CO_2 were identified as the final products whereas acetaldehyde and CO were identified as by-products of ethanol photocatalytic oxidation.

Visible light activity was not detected for TiO_2/MCM-41 and TiO_2/Cr-MCM-41 photocatalysts in oxidation of gas phase diethyl sulfide and ethanol.

1. Introduction

Technologies for removal of air pollutants based on adsorption are well known and widespread due to their simplicity and good efficiency [1]. Due to their high throughput they can be used for high load problems like solvent recovery [2]. However, adsorption is a non-destructive method and toxic adsorbed compounds need further treatment. Thus, methods of chemical destruction have been developed for very toxic compounds like chemical warfare agents (CWA). Popular methods for CWA degradation include perhydrolysis [3], oxidative chlorination, and chemical binding [4,5]. Each chemical method has its own advantages but all of them have one common disadvantage, viz. large amounts of either degassing solutions or toxic gaseous derivatives are formed and require further utilization.

Method of TiO_2 mediated photooxidation of gaseous organic compounds is attracting increasing attention. Photocatalytic oxidation (PCO) over near-UV ($\lambda < 400$ nm) irradiated titanium dioxide has already been tested for the removal of sulfur organic compounds [6,7]. This method leads to relatively non-selective oxidation of practically any organic compound with formation of inorganic species, CO_2, H_2O and inorganic acids, as the final products [8].

The common problems of PCO over TiO_2 are the low quantum efficiency observed and the absence of activity under widespread and cheap solar irradiation. These problems can potentially be solved by doping TiO_2 with transition metals and combining TiO_2 with adsorbents like silica or activated carbon [9]. However, these approaches are mostly studied for liquid phase reactions and their combination has not received much attention [10]. Adsorption capacity and photocatalytic oxidation activity for TiO_2/MCM-41 material was demonstrated previously [11].

In the present study, pure TiO_2 and loaded on MCM-41 doped with chromium was utilized for comparative study on air purification via processes of adsorption and photocatalytic oxidation. Diethyl sulfide (DES) and ethanol were chosen as representatives of organic air pollutants for adsorption and activity measurements under ultraviolet and visible irradiation.

* Corresponding author.
** Corresponding author at: Boreskov Institute of Catalysis, Novosibirsk 630090, Russia. Tel.: +7 3833269447.
E-mail addresses: Panagiotis.Smirniotis@uc.edu (P.G. Smirniotis), voronts@catalysis.ru (A.V. Vorontsov).

1010-6030/$ – see front matter © 2012 Elsevier B.V. All rights reserved.
doi:10.1016/j.jphotochem.2012.01.013

2. Experimental

2.1. Synthesis of TiO_2-loaded Cr-MCM-41 specimens

Cr-modified MCM-41 was synthesized according to the method described previously [12]. The precursor of chromium was $CrCl_3{\cdot}6H_2O$ purchased from Fisher. The Si:Cr atomic ratio was adjusted to 20:1 or 80:1, and the synthesized samples were marked as Cr-MCM-41/20 and Cr-MCM-41/80, correspondingly. In a typical preparation procedure, 35 mL of Ludox HS-40 colloidal silica (40%) was added to 14.6 mL of water under stirring and then 18.2 mL of 40% tetramethylammonium hydroxide (FLUKA) was added. Independently in a separate beaker, 18.25 g of cetyltrimethylammonium bromide (CTABr, Alfa Aesar) was dissolved in 33 mL of water and subsequently 7 mL of 28% aqueous NH_3 was introduced. Finally, these two solutions were mixed. The corresponding amount of $CrCl_3$ was dissolved in water and added dropwise to the resulting mixture. The final mixture was stirred for 30 min and then transferred into a Teflon bottle and treated in an autoclave at 100 °C for 3 days. The obtained slurry was then filtered, washed, dried, and calcined at 550 °C for 10 h in airflow.

To prepare TiO_2-loaded photocatalysts, previously synthesized samples Cr-MCM-41/20, Cr-MCM-41/80 or pure MCM-41 (typically 1.5 g) were dispersed in 100 mL of 2-propanol, and titanium isopropoxide was added to achieve 25% TiO_2 loading. The materials were dried while stirring at ambient temperature and then placed in an oven to dry at 100 °C for 1 h. Finally, the photocatalysts were calcined at 450 °C for 3 h with a temperature ramp 2 °C/min. Synthesized samples are designated TiO_2/Cr-MCM-41/20, TiO_2/Cr-MCM-41/80 and TiO_2/MCM-41.

2.2. Adsorption and photocatalytic activity measurements

Diethylsulfide (DES) (98%) from FLUKA and ethanol (95%) from REACHIM were used as supplied. Adsorption and photocatalytic testing was performed in a 300 cm^3 batch reactor which was installed in the IR Spectrometer Vector 22 (Bruker) cell compartment. The reactor was designed in such a way that one could record IR spectra of either the gas phase or the catalyst surface with adsorbed species without opening the cell [13]. Each IR spectrum was averaged from 32 scans in the 900–4000 cm^{-1} wavenumber region with the 2 cm^{-1} resolution.

The high pressure Hg lamp DRSh-1000 (Russia) was used as the UV light source. Sample irradiation was conducted by condensed light passed through a water filter ($\lambda_{max} \approx 365$ nm, $I = 20$ mW/cm^2). Light intensity was measured by a microvolt meter F-136 (Russia) equipped with a semiconductor light intensity detector calibrated with a ferrioxalate actinometer. A ZhS-11 optical glass filter was placed between the light source and reactor for exclusion of the UV light from lamp spectrum for measuring visible-light activity. The ZhS-11 filter transmission spectrum is presented in Fig. 1.

Samples for photocatalytic activity measurements were prepared as follows. Aqueous suspension of photocatalyst sonicated during 15 min was uniformly deposited onto the CaF_2 glass with diameter 20 mm and thickness 1 mm, and dried at room temperature. The concentration of suspension was chosen so that after drying the density of deposited photocatalyst was ≈1 mg/cm^2. The prepared samples were placed into the thermostated reactor installed in the cell compartment of the FTIR spectrometer. All experiments were conducted using CO_2 and H_2O free air inside the reactor. After placing the photocatalyst sample in the reactor, it was purged with cleaned air at 100 cm^3/min flow rate for 1 h. Then, 0.5 μL of liquid DES or ethanol was injected into the reactor and evaporated at ambient temperature to achieve adsorption equilibrium. The concentration of DES and ethanol vapors in the reactor without adsorption would be 380 and 703 ppm, respectively. Then irradiation of photocatalyst was started and IR spectra of gas-phase and surface were registered at certain intervals.

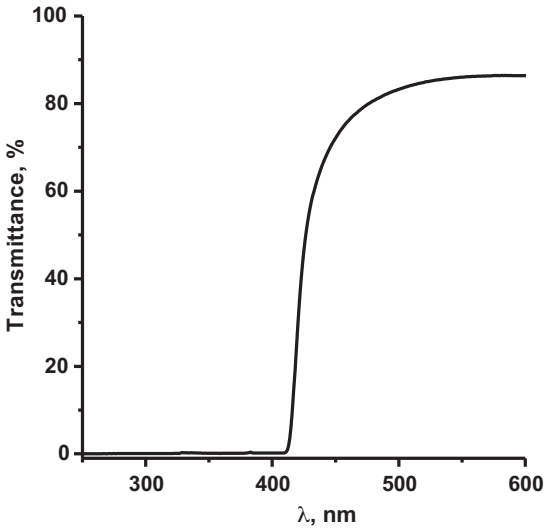

Fig. 1. Transmission spectrum of ZhS-11 optical glass filter used for visible-light experiments.

For adsorption isotherm measurements, 0.2–1.4 μL of DES was injected into the IR cell containing 0.5 g of photocatalyst and the reactor was left for 30 min for the adsorption equilibrium to be established. Then, gas phase FTIR spectrum was registered. The concentration of DES in gas phase was calculated from the area of 2750–3100 cm^{-1} absorption band whereas the CO_2 concentration was calculated from 2200 to 2450 cm^{-1} absorption band using integral form of Beer–Lambert's absorption law. The quantity of the adsorbed DES was calculated from the DES mass balance. Thereafter, additional quantity of liquid DES was injected. The adsorption measurement procedure was repeated several times for obtaining the adsorption isotherms.

3. Results and discussion

3.1. Adsorption of DES

The developed porous structure and high surface area of mesoporous silica materials render them very suitable for adsorption applications. Reduced sulfur compounds are prone to oxidation and the adsorption capacity toward them could be increased by loading adsorbents with oxidizing species. The effect of combining MCM-41 with TiO_2 and Cr^{X+} species on adsorption of DES was investigated by taking DES adsorption isotherms. Fig. 2 shows the isotherms for all the catalysts used in the present study. One can observe that the highest adsorption capacity is observed for Cr-MCM-41/80. Higher loading with Cr and especially loading with TiO_2 decreased the DES adsorption. Adsorption over commercial TiO_2 Degussa P25 and Hombifine N was comparable to that over TiO_2 loaded MCMs.

All the taken isotherms are well described by the Langmuir equation

$$a = \frac{a_m KC}{1 + KC},$$

where a is the amount of DES adsorbed (mol/g), a_m is the monolayer adsorption capacity (mol/g), K is the adsorption constant (ppm^{-1}), C is the equilibrium DES concentration (ppm). The parameters obtained from fitting this equation to the experimental data points are shown in Table 1. This table also lists literature data on the BET surface area, pore volume and pore size of the catalysts.

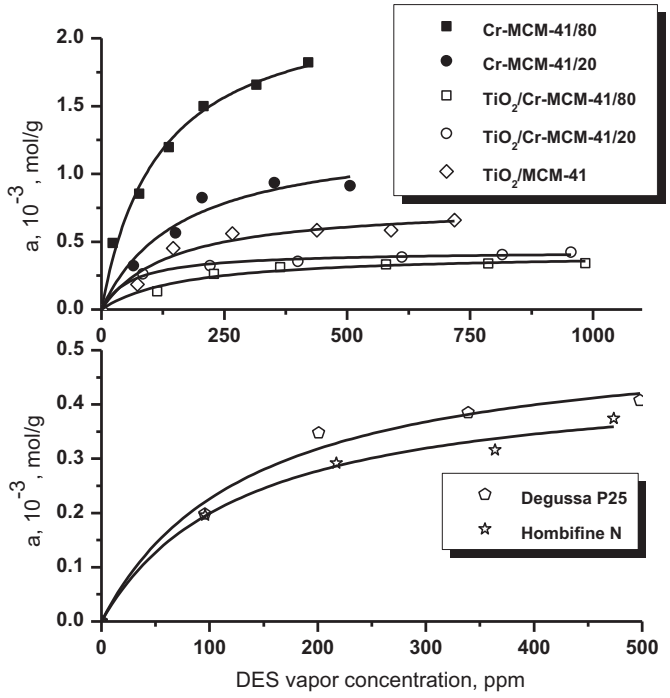

Fig. 2. DES adsorption isotherms at room temperature. Solid lines represent fit of experimental data points with the Langmuir isotherm.

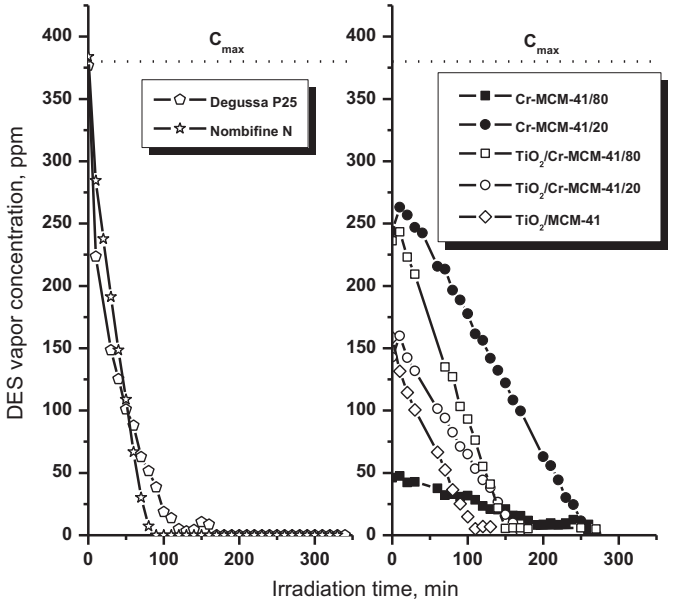

Fig. 3. Kinetic curves of DES vapor removal during PCO in the static reactor under UV irradiation.

The parameters of Langmuir isotherm confirm that Cr-MCM-41/80 has the greatest monolayer capacity and the second high adsorption constant, while TiO_2/Cr-MCM-41/20 exhibited the greatest adsorption constant *K*. Commercially available TiO_2 Hombifine N and Degussa P25 demonstrated lower monolayer capacity but high adsorption constant.

The values of monolayer capacity should demonstrate correlation with the available surface area. There is general correlation among samples with the same preparation procedure. The monolayer capacity per surface area is 2.3 and 2.5 μmol/m^2 for Cr-MCM-41/80 and Cr-MCM-41/20, correspondingly. This means about 0.7 nm^2 area per each DES molecule in monolayer. The TiO_2 loaded samples have capacity of 0.54 and 0.74 μmol/m^2 for/80 and/20 samples, and 0.87 μmol/m^2 for TiO_2/MCM-41. Interestingly, the highest monolayer capacity per surface area was obtained over TiO_2 P25 and is equal to 8.2 μmol/m^2. This can be associated with the fire preparation method of this TiO_2 and possibly high availability of surface five-coordinated titanium sites Ti_{5C}.

3.2. Photodegradation of DES

Adsorption provides only phase change of air pollutants from gas phase into the adsorbed state. Complete destruction into innocuous products is desirable for safe disposal of spent adsorbent. Thus, photocatalytic oxidation of DES was performed over all the catalysts under the current study. After the injection of liquid DES, the reactant evaporated and the gas phase concentration equilibrated for 30 min. Without adsorption effects, the initial DES concentration would be 380 ppm. After the adsorption of DES has been established, UV irradiation started and the changes in DES and oxidation products concentration were traced with FT-IR spectroscopy. Fig. 3 shows changes in the gas phase concentration of DES during PCO. The kinetic curves for different catalysts are different in two respects. The initial concentration is different due to different parameters of adsorption isotherm over the catalysts. The highest initial concentration is observed over commercial TiO_2 Degussa P25 and Hombifine N. The lowest initial concentration is observed for Cr-MCM-41/80 in accord with its highest monolayer capacity and high adsorption constant (Table 1).

The second difference is in the slope of the DES concentration kinetic curves which is determined by the rate of DES consumption in the initial oxidation step. The initial part of the curve during at least 50 min is well described by a linear function for the catalysts studied. Table 2 gives the values of DES removal rate from gas phase in the second column. The highest rate of DES removal is observed for TiO_2 Hombifine N and the second high is for Degussa P25. Among the MCM based materials, the highest DES consumption rate is for TiO_2/Cr-MCM-41/80 sample. This is in accord with its higher surface area compared to TiO_2/Cr-MCM-41/20. The surface area is essential for DES removal during the first stage of photocatalytic oxidation as demonstrated earlier [6].

Table 1
Adsorption and textural properties of photocatalysts under investigation.

Catalyst	DES adsorption approximated with Langmuir isotherm, T = 298 K		Nitrogen adsorption		
	a_m (mmol/g)	K ($\times 10^{-3}$ ppm^{-1})	S_{BET} (m^2/g)	Pore volume (cm^3/g)	Pore size (Å)
Cr-MCM-41/80	2.3	8.44	999	0.99	40
Cr-MCM-41/20	1.67	3.88	664	1.14	69
TiO_2/Cr-MCM-41/80	0.42	5.93	777	0.65	32
TiO_2/Cr-MCM-41/20	0.41	20.14	547	0.81	57
TiO_2/MCM-41	0.77	7.27	890	0.77	32
Hombifine N	0.57	7.28	341	–	–
Degussa P25	0.46	7.71	56	0.25	175

The morphology data calculated from nitrogen adsorption isotherm was taken from [20] except the data for Degussa P25 which were taken from [21].

Table 2
Activity of different catalysts in DES oxidation under UV light.

Catalyst	DES initial removal rate (ppm/min)	CO_2 formation rate	
		Initial (ppm/min)	Average (ppm/min)
Cr-MCM-41/80	0.20	0.27	0.16
Cr-MCM-41/20	1.0	0.48	0.32
TiO_2/Cr-MCM-41/20	0.99	0.35	0.275
TiO_2/Cr-MCM-41/80	1.7	0.07	0.056
TiO_2/MCM-41	1.4	0.19	0.202
TiO_2 Hombifine N	**4.9**	0.20	**1.1**
TiO_2 P25	**3.9**	0.18	**3.6**

The initial rates were calculated for the first 30 min of irradiation. The bold values indicate the highest value.

Then, we compare the characteristic time of air purification based on the intersect point of the linear initial kinetic curve with the abscises axis. In this manner, we find that commercial TiO_2 samples purify air in ~100 min, and TiO_2/MCM-41 purifies air in 110 min. TiO_2/Cr-MCM-41/80 sample purifies air from DES in 150 min. As shown above, the greatest adsorption capacity was observed for Cr-MCM-41/80. However, its activity for DES destruction was the lowest among the systems tested. One of the possible explanations of such behavior is the strong adsorption of the reactant which hinders DES molecules from subsequent transfer onto the photocatalytically active sites of Cr-MCM-41/80 material. By studying catalysts with other transition metals, it has been shown that this catalyst shows the greatest activity in oxidation of 4-chlorophenol in aqueous solution under UV-light and shows activity under visible light [14]. In gas phase, the activity under visible light was not detected, which justifies that different mechanisms are operational in gas and liquid phase photocatalytic oxidation. It should be noted that all the studied catalysts are capable of complete air purification from DES vapor via photocatalytic oxidation. It is especially interesting phenomenon for samples Cr-MCM-41/80 and/20 since they do not contain TiO_2.

For additional correct comparison of the different photocatalysts, it is necessary to consider the process of DES deep oxidation into CO_2, water and surface sulfates. Fig. 4 demonstrates the CO_2 concentration kinetic curves taken during DES PCO. The curves demonstrate strongly non-linear character but one can always take several initial points for calculating the initial rate. Table 2 presents the initial and average rate of CO_2 production (third and fourth columns, respectively). The highest CO_2 production rate is for P25 and the CO_2 concentration reaches a plateau value of 680 ppm at about 200 min. TiO_2 Hombifine N is also very active. The high photocatalytic activity of TiO_2 P25 is explained by the synergistic effect of anatase and rutile allotropic forms present in this material, an effect described in the literature [15]. For the deep DES oxidation, its higher compared to TiO_2 Hombifine N activity should be ascribed to higher stability of TiO_2 P25 surface toward deactivation by oxidation products and higher selectivity to complete oxidation. The combustion high temperature preparation method of P25 makes its surface stable to chemical dissolution by H_2SO_4 which is complete oxidation product of DES.Among the MCM-based photocatalysts, the highest CO_2 evolution rate is observed over Cr-MCM-41/20. Its high activity may be due to the strong oxidizing power of Cr species present in the MCM framework in the highest content. Deposition of TiO_2 decreases activity and the lowest CO_2 production rate is observed over TiO_2/Cr-MCM-41/80 while it possesses the highest rate of DES vapor removal. Obviously, Cr^{6+} ions induce significant photocatalytic activity in MCM-41 containing samples and this activity is proportional to the Cr content. This can be explained by the fact that TiO_2/Cr-MCM-41/80 has larger surface area compared to TiO_2/Cr-MCM-41/20, but the amount of Cr^{6+} in the latter is higher which leads to an increase in the rate of carbon dioxide formation [16]. The results on ethanol oxidation presented lower confirm that Cr-MCM-41/20 is a balanced photocatalyst with high activity in adsorption, initial stage of photocatalytic oxidation and deep oxidation into inorganic products.Besides the final gaseous products CO_2 and H_2O, we also detected DES partial oxidation products, namely ethylene and acetaldehyde. They result from the oxidation of adsorbed DES molecule with photogenerated holes that finally can be converted into carbon dioxide [17].

The surface processes during PCO can be conveniently traced by using absorption spectra of photocatalysts. Fig. 5 demonstrates absorption spectra of TiO_2 Hombifine N taken at half hour intervals during the 240 min of DES PCO in the low frequency region. Initially, only low intensity bands at 1380, 1517 and 1641 cm^{-1} are observed on pure TiO_2. They correspond to adsorbed water

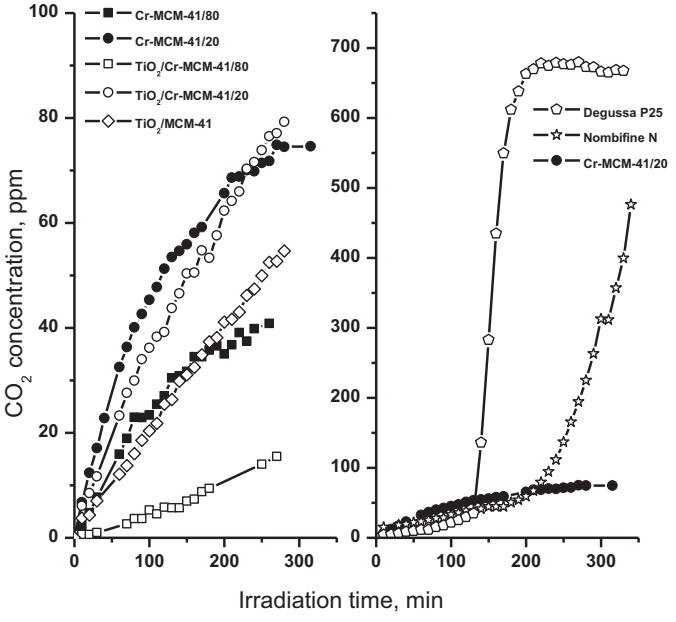

Fig. 4. Kinetic curves of CO_2 accumulation in PCO of DES in the static reactor under UV irradiation.

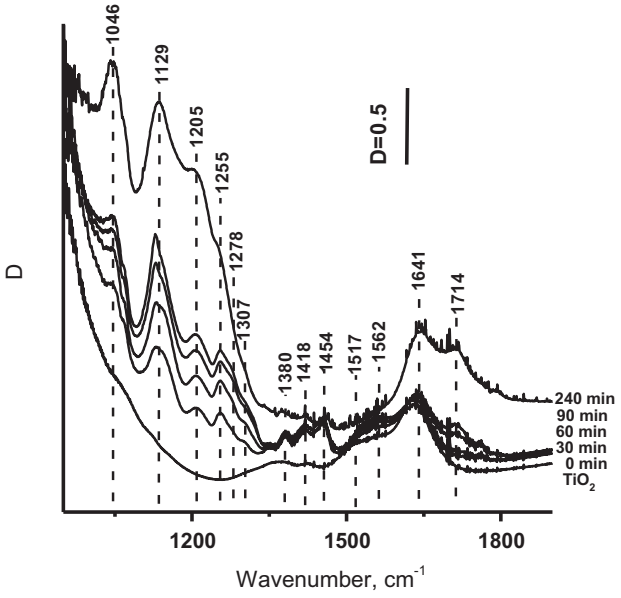

Fig. 5. Evolution of the FTIR absorption spectrum of the TiO_2 Hombifine N during PCO of DES under UV light. *D* is absorbance.

Table 3
IR spectral features and their assignment for DES photooxidation over TiO_2.

Absorption bands (cm^{-1})		Assignment	Ref.
P25	Hombifine N		
1048	1046	Monodentate sulfate	[22,23]
1126	1129	Monodentate and bidentate sulfate	
1210	1205	Carbonate	
1257	1255	DES δ(—CH_2—S—)	
–	1278	DES CH_2 wagging	
1306	1307	Carbonate	
1381	1380	δ_s(CH)	[24]
1419	1418	Carboxyl ν_s(O—C—O)	
1451	1454	$\delta(CH_2)$, $\delta_{as}(CH_3)$	
–	1517	Carboxyl species ν_s(C—O—O)	[17]
–	1562	Carboxyl species ν_{as}(C—O—O)	[22]
1628	1641	H_2O	[17,22]
1715	1714	Carbonyl ν(C=O)	[22,24]

and impurities such as carbonates and carboxylates arising from the photocatalytic oxidation of traces of adsorbed organic species and sulfates arising from TiO_2 synthesis precursor $TiO(SO_4)$. Admission of DES results in generation of absorption bands at 1046, 1129, 1205, 1255, 1380, 1418, 1454, and 1562 cm^{-1}. These bands correspond to adsorbed DES and to products of its partial oxidation. After the oxidation process comes to its conclusive stage at 420 min, one can observe intensive absorption bands at 1046, 1129, 1205, 1641 and 1714 cm^{-1}. The assignment of these bands has been carried out using literature data and is given in Table 3.

Since the CO_2 production kinetics is different over TiO_2 P25, the surface changes have been recorded for this sample as well. Fig. 6 shows how the TiO_2 IR spectrum changes during the DES PCO. Compared to TiO_2 Hombifine N, the absorption band intensity is lower for TiO_2 P25 primarily due to the smaller quantity of intermediates as a result of the smaller surface area of the latter photocatalyst. The organic intermediates such as carboxyl species (1517 and 1562 cm^{-1}) are present on TiO_2 P25 in much smaller quantities and this is related to their faster oxidation into inorganic products. Therefore, the activity of P25 is above that of Hombifine N though in many other cases of gas phase PCO the highest activity is observed for Hombifine N.

Accumulation of surface sulfates was observed during photooxidation leading to the catalyst deactivation. Earlier it was shown that

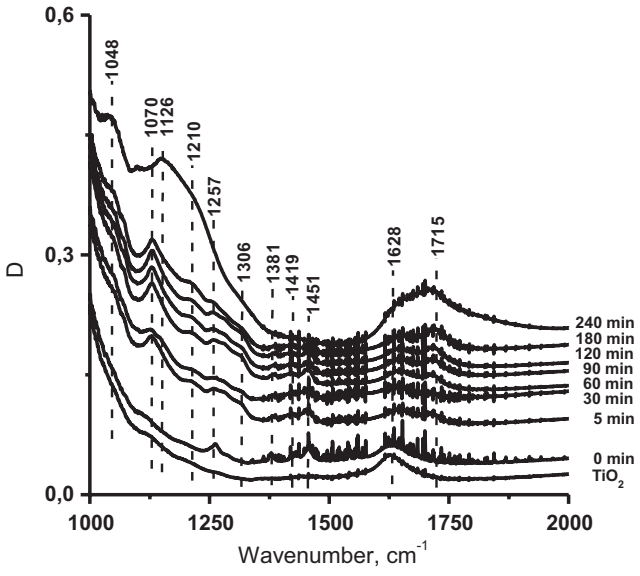

Fig. 6. Evolution of the FTIR spectrum of TiO_2 P25 during PCO of DES under UV light. *D* is the absorbance.

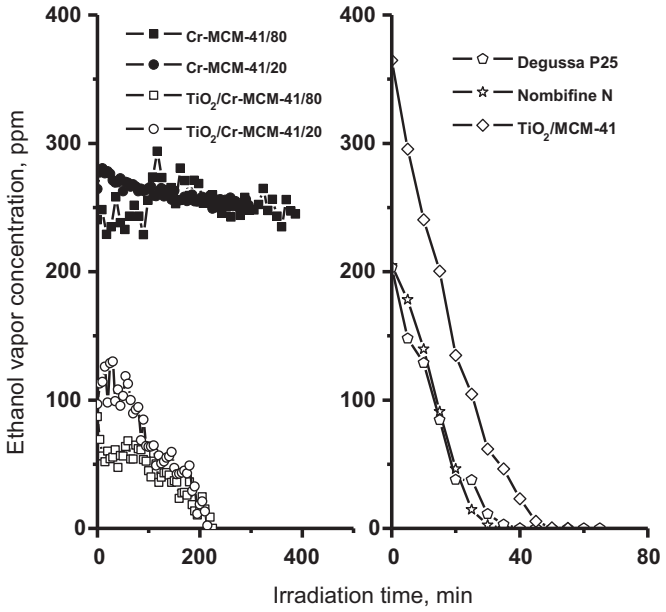

Fig. 7. Kinetic curves of ethanol concentration during the ethanol PCO under UV light in the static reactor.

sulfates can lead to reduction of activity of the catalyst as a whole. However, the deactivation was reversible since the produced sulfates were removed by washing the catalyst surface with water and thus completely restoring the photocatalyst's activity [18]. Irradiation of any of the photocatalysts with visible light did not result in any notable consumption of DES or formation of oxidation products.

3.3. Photodegradation of ethanol

Ethanol molecule is very easy to be oxidized and serves as an electron donor in photocatalytic processes. Its complete and partial oxidation has been demonstrated for many ultraviolet and visible light active photocatalysts, respectively. Therefore, it was interesting to compare the oxidation of DES and ethanol vapors for all the studied photocatalysts. For each test, liquid ethanol was injected into the IR cell, evaporated and equilibrated with the photocatalyst for 30 min. Then, irradiation started and continued for 5–8 h. Fig. 7 shows changes in ethanol concentration during PCO. Table 4 summarizes the rates of ethanol consumption and carbon dioxide formation. The highest rate of ethanol consumption is observed for TiO_2/MCM-41 photocatalyst, while the commercial TiO_2 photocatalysts P25 and Hombifine N demonstrated comparable but lower activity. This contrasts drastically from the DES PCO rates. Chromium species possibly play inferior role in

Table 4
Activity of catalysts in ethanol photooxidation.

Catalyst	EtOH initial consumption rate (ppm/min)	CO_2 formation rate	
		Initial (ppm/min)	Average (ppm/min)
Cr-MCM-41/80	0.098	0.082	0.038
Cr-MCM-41/20	0.078	0.051	0.007
TiO_2/Cr-MCM-41/20	2.4	0.255	0.29
TiO_2/Cr-MCM-41/80	1.1	0.24	0.41
TiO_2/MCM-41	**10**	**2.6**	**5.2**
TiO_2 Hombifine N	**7.3**	**21.5**	**27.2**
TiO_2 P25	**6.3**	**8.3**	**20**

The initial rate values were calculated for the first 30 min of reaction. The bold values indicate the highest value.

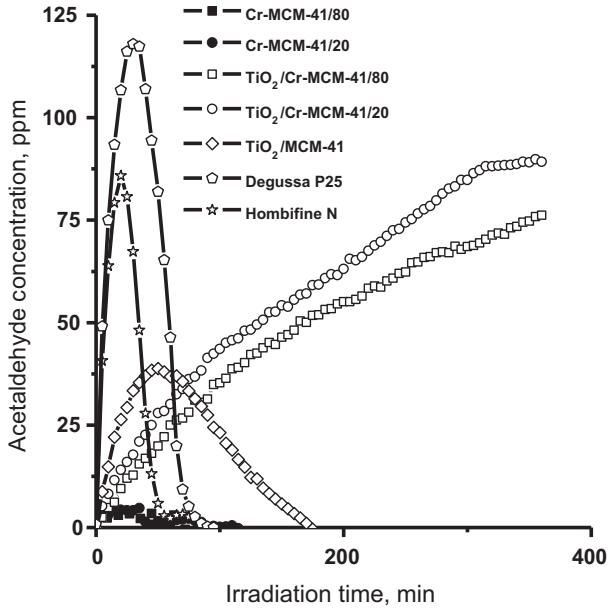

Fig. 8. Kinetic curves of acetaldehyde concentration during the ethanol PCO under UV light.

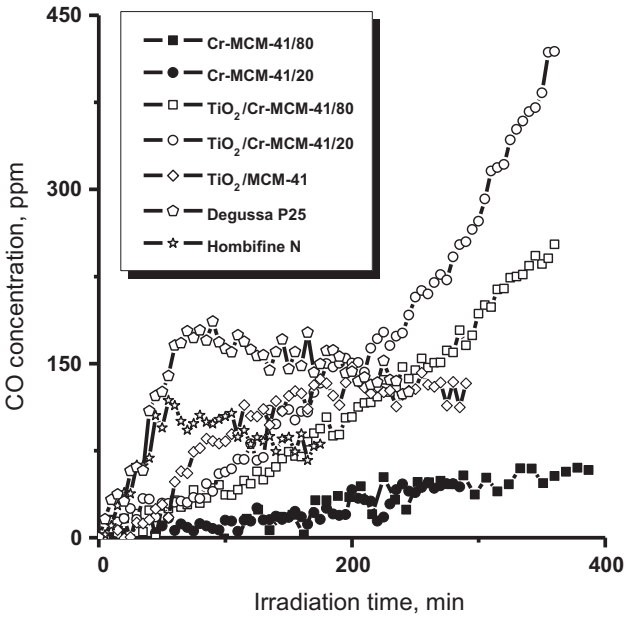

Fig. 9. Kinetic curves of CO formation during ethanol PCO under UV light.

ethanol oxidation contrasting to DES oxidation. TiO_2 seems to be essential for ethanol oxidation and the catalysts without TiO_2, Cr-MCM-41/80 and Cr-MCM-41/20, showed only very low activity. Bhattacharya et al. [19] showed that activity in the oxidation of methanol on similar catalysts depends on the content of TiO_2 in the samples TiO_2/M-MCM-41, crystallite size and surface area. Their results also show that the effect of TiO_2 crystallite size in the photo-catalytic properties relate mainly to the larger surface area and hence to the enhanced number of chemisorption sites, rather than to the changes in electronic properties. Therefore, the most active catalyst in the deep oxidation of ethanol is Hombifine N.

Acetaldehyde is the partial oxidation intermediate product that often appears in ethanol photocatalytic oxidation in gas phase. This compound appeared during ethanol PCO over all the photocatalysts in the present study. Fig. 8 demonstrates acetaldehyde concentration kinetic curves. The curves have a bell-shaped form typical for intermediate products for all catalysts except the TiO_2/Cr-MCM-41 samples which probably have too low activity for further oxidation of acetaldehyde. This is confirmed by comparing Figs. 7 and 8. After 300 min of reaction, the ethanol concentration decreased below detection limit but evolution of acetaldehyde continued and consumption did not proceed. Thus, oxidation of acetaldehyde into deeper oxidation products is a slow process compared to acetaldehyde generation. The slope of the acetaldehyde consumption part of kinetic curve is indicative of acetaldehyde consumption rate. For commercial TiO_2 samples the rate is close to each other while for TiO_2/MCM-41 the rate is lower. The acetaldehyde production is faintly seen for Cr-MCM-41 samples.

Analysis of IR spectra of gas phase inside the cell showed that carbon monoxide was formed during ethanol PCO. The CO concentration was quantified for all the photocatalysts tested and is shown in Fig. 9. The highest CO build up is observed for the TiO_2/Cr-MCM-41/20 photocatalyst. For commercial TiO_2 Degussa P25 and Hombifine N, CO concentration reaches maximum values after approximately 80 min of irradiation. Then, CO is consumed and transformed into CO_2. However, for the MCM-41 based photocatalysts, CO consumption was not noted probably because of their low activity.

The final oxidation products of ethanol are carbon dioxide and water. While it is difficult to trace the concentration of water due to its high adsorption on the photocatalyst surface, it is easy to measure the CO_2 concentration. Fig. 10 reveals the CO_2 concentration kinetic curves for all the photocatalysts. Table 4 gives the values of the CO_2 formation rates. The highest deep oxidation rate is observed over TiO_2 Hombifine N. The CO_2 concentration reaches a plateau at about 85 min of UV irradiation. TiO_2 P25 is only slightly less active. Photocatalyst TiO_2/MCM-41 is also capable reaching plateau of CO_2 concentration at time 200 min, but the plateau concentration is lower because some carbon stays in carbon monoxide and possibly as species adsorbed over non-irradiated parts of this photocatalyst. Photocatalysts without TiO_2 loading demonstrated very low activities in contrast to the DES PCO case. Thus, the MCM-41 photocatalysts proved to be active photocatalysts but their composition and properties should be further adjusted for attaining the PCO activity standards set by commercial TiO_2 photocatalysts.

We also tested our catalysts in the ethanol oxidation under visible light. They have not shown photocatalytic activity during

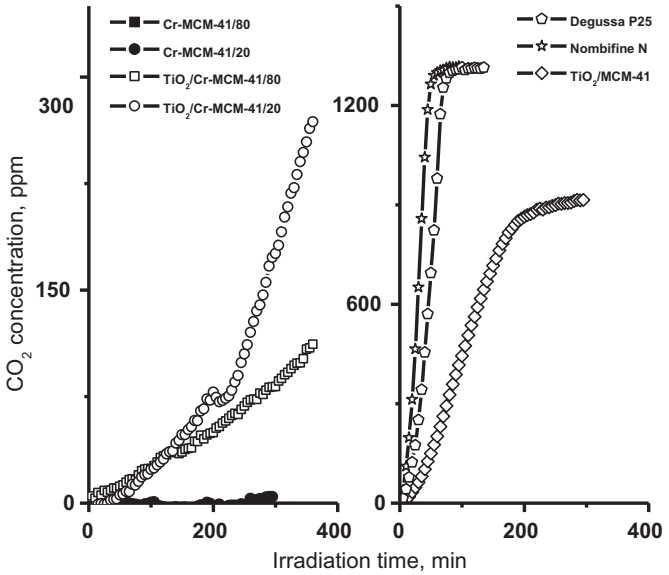

Fig. 10. Kinetic curves of CO_2 concentration during ethanol PCO under UV light.

diethyl sulfide oxidation under visible light but ethanol should be oxidized under visible light easier than diethyl sulfide. However, ethanol oxidation was not revealed at all. Probably it can be explained by cutting a large part of light by ZhS-11 filter so that the irradiance left was too low (130 mW/cm^2).

4. Conclusions

Adsorption and oxidation of DES on various catalysts have been studied. We observed the complete removal of DES vapor from the gas phase after 200 min and this removal took less than 100 min on the most active catalyst P25. Catalysts on the basis of MCM-41 removed DES vapor due to the high adsorption capacities whereas commercial catalysts possess greater photocatalytic activity. Therefore, use of catalysts on the base of supported MCM-41 and commercial TiO_2 catalysts is possible. During PCO water, carbon dioxide, surface sulfates and other species were formed. Ethanol is fast oxidized on commercial catalysts and forms two gaseous byproducts carbon oxide and acetaldehyde.

Acknowledgments

The support of the Ministry of Education and Science of Russia via contract 16.513.11.3091, SB RAS Integration projects 70 and 36, Presidium RAS grant 27.56, NATO SfP-981461 project as well as the Federal Special Program "Scientific and Educational Cadres of Innovative Russia" (2009–2013 years) via contract P1360, and President RF grant NSh-524.2012.3 is gratefully acknowledged.

References

[1] J.S. Waston, Separation Methods for Waste and Environmental Applications, Marcel Dekker, New York, 1999, pp. 23–32.
[2] M.J. Ruhl, Recover VOCs via adsorption onto activated carbon, Chem. Eng. Prog. 89 (1993) 37–41.
[3] Y.-C. Yang, F.J. Berg, L.L. Szafraniec, W.T. Beaudry, C.A. Bunton, A. Kumar, Peroxohydrolysis of nerve agent VX and model compounds and related nucleophilic reactions, J. Chem. Soc. Perkin Trans. 2 (1997) 607–613.
[4] Y.-C. Yang, J.A. Baker, J.R. Ward, Decontamination of chemical warfare agents, Chem. Rev. 92 (1992) 1729–1743.
[5] S. Franke, P. Franz, W. Warnke, Lehrbuch der Militärchemie, Deutscher Militärverlag, Berlin, 1967.
[6] A.V. Vorontsov, E.V. Savinov, L. Davydov, P.G. Smirniotis, Photocatalytic destruction of gaseous diethyl sulfide over TiO_2, Appl. Catal. B: Environ. 32 (2001) 11–24.
[7] A.V. Vorontsov, Russ. Chem. Rev. 77 (2008) 909–926.
[8] O. Carp, C.L. Huisman, A. Reller, Photoinduced reactivity of titanium dioxide, Prog. Solid State Chem. 32 (2004) 33–177.
[9] W. Zhang, L. Zou, L. Wang, Photocatalytic TiO_2/adsorbent nanocomposites prepared via wet chemical impregnation for wastewater treatment: a review, Appl. Catal. A: Gen. 371 (2009) 1–9.
[10] L. Zang, W. Macyk, C. Lange, W.F. Maier, C. Antonius, D. Meissner, H. Kisch, Visible-light detoxification and charge generation by transition metal chloride modified titania, Chem. Eur. J. 6 (2000) 379–384.
[11] Y. Xu, C.H. Langford, Photoactivity of titanium dioxide supported on MCM41, zeolite X, and zeolite Y, J. Phys. Chem. B 101 (1997) 3115–3121.
[12] L. Davydov, E.P. Reddy, P. France, P.G. Smirniotis, Transition-metal-substituted titania-loaded MCM-41 as photocatalysts for the degradation of aqueous organics in visible light, J. Catal. 203 (2001) 157–167.
[13] D.A. Trubitsyn, A.V. Vorontsov, Experimental study of dimethyl methylphosphonate decomposition over anatase TiO_2, J. Phys. Chem. B 109 (46) (2005) 21884–21892.
[14] E.P. Reddy, B. Sun, P.G. Smirniotis, Transition metal modified TiO_2-loaded MCM-41 catalysts for visible- and UV-light driven photodegradation of aqueous organic pollutants, J. Phys. Chem. B 108 (2004) 17198–17205.
[15] R.I. Bickley, T. Gonzalez-Carreno, J.S. Less, L. Palmisano, R.J.D. Tilley, A structural investigation of titanium dioxide photocatalysts, J. Solid State Chem. 92 (1991) 178–190.
[16] R. Portela, M.C. Canela, B. Sanchez, F.C. Marques, A.M. Stumbo, R.F. Tessinari, J.M. Coronado, S. Suarezet, H_2S photodegradation by TiO_2/M-MCM-41 (M = Cr or Ce): deactivation and by-product generation under UV-A and visible light, Appl. Catal. B: Environ. 84 (2008) 643–650.
[17] D.V. Kozlov, A.V. Vorontsov, P.G. Smirniotis, E.N. Savinov, Gas-phase photocatalytic oxidation of diethyl sulfide over TiO_2: kinetic investigations and catalyst deactivation, Appl. Catal. B: Environ. 42 (2003) 77–87.
[18] D.A. Panayotov, D.K. Paul, J.T. Yates Jr., Photocatalytic oxidation of 2-chloroethyl ethyl sulfide on TiO_2–SiO_2 powders, J. Phys. Chem. B 107 (2003) 10571–10575.
[19] K. Bhattacharya, A.K. Tripathi, G.K. Dey, N.M. Gupta, Vapor-phase photooxidation of methanol over nanosize titanium dioxide clusters dispersed in MCM-41 host material. Part 1: synthesis and characterization, J. Nanosci. Nanotechnol. 5 (2005) 797–805.
[20] B. Sun, E.P. Reddy, P.G. Smirniotis, TiO_2-loaded Cr-modified molecular sieves for 4-chlorophenol photodegradation under visible light, J. Catal. 237 (2006) 314–321.
[21] K. Joseph, A. Raj, B. Viswanathan, Effect of surface area, pore volume and particle size of P25 titania on the phase transformation of anatase to rutile, Ind. J. Chem. A 48 (2009) 1378–1382.
[22] B. Smith, Infrared Spectral Interpretation: A Systematic Approach, CRC Press, 1999.
[23] K. Nakamoto, Infrared and Raman Spectra of Inorganic and Coordinated Compounds, Wiley, New York, 1986.
[24] G. Socrates, Infrared Characteristic Group Frequencies, Wiley, New York, 1994.